Features of crevasse splay deposits and sedimentary processes associated with levee breaching by the October 2019 flood of the Chikuma River, Central Japan

Masaki Yamada [a,*], Hajime Naruse [b], Yugo Kuroda [a], Taichi Kato [c], Yuhei Matsuda [d], Tetsuya Shinozaki [e], Tetsuya Tokiwa [a]

[a] *Department of Geology, Faculty of Science, Shinshu University, 3-1-1 Asahi, Matsumoto, Nagano 390-8621, Japan*
[b] *Division of Earth and Planetary Sciences, Graduate School of Science, Kyoto University, Kitashirakawa-Oiwakecho, Sakyo-ku, Kyoto, Kyoto 606-8502, Japan*
[c] *Geology Unit, Science Division, Department of Science, Graduate School of Science and Technology, Shinshu University, 3-1-1 Asahi, Matsumoto, Nagano 390-8621, Japan*
[d] *Department of Mathematics, Faculty of Science, Shinshu University, 3-1-1 Asahi, Matsumoto, Nagano 390-8621, Japan*
[e] *National Museum of Japanese History, 117 Jonai-cho, Sakura, Chiba 285-8502, Japan*
[*]Corresponding author. *E-mail address:* yamada@shinshu-u.ac.jp (M. Yamada).

ABSTRACT

Field investigations and analyses of modern crevasse splay deposits can both elucidate the processes of levee breaching and help to identify past crevasse splay deposits from geologic strata, thereby estimating the magnitudes of ancient river floods. In this study, we studied levee breach processes and crevasse splay deposits in order to determine the distribution characteristics of the inundation area associated with the 2019 flooding of the Chikuma River, Central Japan. The crevasse splay formed by this event can be divided into three regions: proximal, medial, and distal splays. Behind the breached levee, sandy and gravelly sediment piles (proximal splay) formed at both sides of the crevasse channel, whereas sand and mud layers (medial and distal splays) were observed over a wide area within the inundation area, extending beyond the sediment piles. The upstream gravelly sediment pile (proximal splay) was characterized by clearly bounded lower sand and upper gravel layers, reflecting the process of levee breaching: the outer sandy soil of the artificial levee began to be scoured by external erosion, followed by the erosion of the inner gravelly soil. The sedimentary characteristics of the proximal splay deposits appear to have been strongly controlled by the local environment but are useful for inverse analysis of the progressive process of past and future levee breaches. Sandy crevasse splay deposits (medial splay) thinned rapidly away from the breached levee, whereas muddy crevasse splay deposits (distal splay) were thicker at lower elevations, indicating that they formed during the levee breach and stagnant stages, respectively. The distribution of the medial splay (35.7% of the inundation area) was restricted relative to that of the distal splay (~81.7% of the inundation area). This study indicates that it is important to determine the extent of muddy crevasse splay deposits from geologic strata in order to determine the inundation areas of past levee breaches.

Keywords: River flood; Levee breach; Crevasse splay deposit; Maximum extent

1. Introduction

Natural disasters created by flooded rivers can cause enormous damage. In recent years, large-scale river floods have occurred almost every year worldwide, causing extensive damage across river basins (e.g., Shakti et al., 2020; Fekete and Sandholz, 2021). Typhoon No. 19 (Hagibis) on October 6–13, 2019, was one of the strongest typhoons witnessed in Japan for several decades, and led to widespread damage across mainland Japan (e.g., Yamamoto et al., 2020; Tinh et al., 2021; Tsuchiya, 2021). Heavy rainfall associated with this typhoon resulted in at least 135 levee breaches across 71 rivers (Tinh et al., 2021), including the 367 km long Chikuma River (Nagano Prefecture) and Shinano River (Niigata Prefecture), located in Central Japan, the region of interest for this study (Fig. 1A).

River flooding inundates adjacent floodplains and deposits large amounts of sediment, forming a volumetrically significant part of alluvial and deltaic overbank deposits (e.g., Allen, 1965; Hughes and Lewin, 1982; O'brien and Wells, 1986; Nanson and Croke, 1992; Bristow et al., 1999; Colombera et al., 2013; Burns et al., 2017). River flooding events can be divided into two major types: levee overflows and levee breaches, with the latter generally being larger in magnitude. Deposits formed by levee breaching events are termed crevasse splays, and typically form fan- or lobe-shaped sediment mounds (Smith et al., 1989; Burns et al., 2017; Rahman et al., 2022a). Many studies have been conducted on the structure, size, and morphology of the crevasse splays in order to understand the causes and effects of modern floods and similar ancient deposits preserved in geologic strata (e.g., O'brien and Wells, 1986; Mjøs et al., 1993; Bristow et al., 1999; Pérez-Arlucea and Smith, 1999; Jones and Hajek, 2007; Arnaud-Fassetta, 2013; Burns et al., 2017; Colombera and Mountney, 2021; Rahman et al., 2022a, b; Widera et al., 2023). Although many studies of modern crevasse splays have been conducted in areas where large meandering rivers have developed, most have investigated morphological changes on a scale of several years to several decades (e.g., Bristow et al., 1999; Pérez-Arlucea and Smith, 1999; Farrell, 2001; Buehler et al., 2011; Cahoon et al., 2011; Li and Bristow, 2015; Toonen et al., 2016). Hence, studies detailing the crevasse splay deposits formed by individual levee breaching events and discussing their formation process have typically been quite limited (Gębica and Sokołowski, 2001; Nelson and Leclair, 2006; Hori and Hirouchi, 2011; Arnaud-Fassetta, 2013; Matsumoto et al., 2016; Sato et al., 2017). Additionally, engineering studies based on field investigations and numerical calculations have been conducted to clarify the mechanism of levee breaches (e.g., Viero et al., 2013; Orlandini et al., 2015; Özer et al., 2020), but few studies have reconstructed the levee breaching process based on the sedimentary facies of crevasse splay deposits (Matsumoto et al., 2016; Sato et al., 2017).

Matsumoto et al. (2016) and Sato et al. (2017) investigated crevasse splay deposits formed by the 2015 flood of the Kinu River, Central Japan, but focused only on the main crevasse splay bodies and did not examine the distribution and sedimentary characteristics of deposits throughout the inundation area. Accumulating data on the distribution characteristics of crevasse splay deposits covering the entire inundation area should enable the origin and magnitude of extreme event deposits recorded in geologic strata to be accurately identified (Burns et al., 2017).

This study uses river water level data and drone images, in addition to sedimentological and hydrological surveys, covering the entire inundation area of a levee breach in order to elucidate the processes of levee breaching and sedimentation with heretofore unprecedented detail. For the 2019 flood of the Chikuma River, sedimentological studies on crevasse splay deposits have not been reported, although surveys of damage to levee revetments and floodplains have been conducted (Investigation Committee on the Chikuma River Levee, 2020; Yamamoto et al., 2020; Ohtsuka et al., 2021; Tsuchiya, 2021). In addition, gravelly crevasse splay deposits were formed in this study site; these have not been observed in previous cases (Hori and Hirouchi, 2011). Most reported crevasse splay deposits, both modern and ancient, are sandy (e.g., Gębica and Sokołowski, 2001; Nelson and Leclair, 2006; Arnaud-Fassetta, 2013; Matsumoto et al., 2016; Sato et al., 2017). Thus, determining the sources and depositional processes of gravelly crevasse splay deposits will enhance our understanding of levee breaches and their resulting deposits.

2. Study area

2.1. Geomorphological setting

The Chikuma River originates in eastern Nagano Prefecture and flows northward into the Sea of Japan, running southwest to northeast through the study area (Fig. 1A). The channel width at the study site is approximately 230 m during low-water conditions and 900 m during high-water conditions (Fig. 2). The high-water channel was mainly used for apple orchards prior to the flooding event. Residential dwellings, cultivated areas, and apple orchards are located on the floodplain developed between the river and the highlands. National Route 18, an elevated railway, and two branch streams cut across the floodplain (Fig. 3A).

2.2. October 2019 flooding event

Heavy rainfall on October 12, 2019, associated with Typhoon No. 19 (Hagibis), caused overflows in many places, including along the Chikuma River (Fig. 1A). Typhoon No. 19 developed around Minamitorishima Island in the Pacific Ocean (15.1°N, 158.2°E) at 3:00 am on October 6 and reached Izu Peninsula at 7:00 pm on October 12, 2019, with a central pressure of 955 hectopascals (Fig. 1A; Japan Meteorological Agency, 2019). The total amount of rainfall exceeded 500 mm in the upstream region of the Chikuma River.

On the midstream left bank of the Chikuma River (the study area), closed-circuit Television (CCTV) camera installed on the breached levee (Fig. 2A and B) indicated that river water overflowed the levee at 0:55 am on October 13 (Investigation Committee on the Chikuma River Levee, 2020) (Fig. 4). The last image acquired by the CCTV camera was taken at 2:15 am, and the Chikuma River Office made an urgent announcement about the levee breach at 5:30 am, i.e., the levee breach occurred between 2:15 am and 5:30 am on October 13 (Fig. 4). The 30 m wide left bank levee revetment was breached over a length of 70 m (Figs. 2B, 5A, and 6A), resulting in inundation of the 6 km wide floodplain up to a distance of 2.23 km from the breached levee (Fig. 3B). The area of the overflow is estimated to have reached up to 400 m upstream and up to 900 m downstream from the breached levee (Fig. 3B; Investigation Committee on the Chikuma River Levee, 2020).

2.3. Internal structure of the levee revetment

The Investigation Committee on the Chikuma River Levee (2020) and Ohtsuka et al. (2021) estimated the composition of the levee revetment based on the breached upstream and downstream sections. The lower and middle parts of the levee consisted of sandy soil (1–2 m thick) and gravel (~2.5 m thick), respectively, whereas the upper part of the levee was composed of cohesive soil (~2 m thick) (Fig. 6B; Investigation Committee on the Chikuma River Levee, 2020). The landside along the levee flank led to a 2–3 m thick cover of sandy soil through an area planted with cherry trees. The surface of the levee was paved with asphalt concrete (Fig. 6C and D). Based on the observation of the breached sections, the upstream section contained large amounts of gravelly soil, whereas the main constituent of the downstream section is sandy soil, i.e., the composition of the levee revetment differs between the breached upstream and downstream sections (Investigation Committee on the Chikuma River Levee, 2020; Ohtsuka et al., 2021).

The Investigation Committee on the Chikuma River Levee (2020) also estimated the volume of sediments released from the breached levee on the basis of cross-sectional levee observations. The total volume of released sediments was approximately 20,560 m^3, of which 3,400 m^3, 12,180 m^3, and 4,980 m^3 were gravelly, sandy, and cohesive soils, respectively.

3. Methods

3.1. Field surveys

We conducted a comprehensive field survey covering the entirety of the inundation area (Fig. 3); detailed investigations were also conducted around the area of the breached levee (Fig. 5).

3.1.1. Survey covering the entire inundation area

Field surveys covering the entire inundation area were conducted in order to establish the thickness and grain size distribution of the crevasse splay deposit for 14 days between October 18 and November 28, 2019. We set up a 2.23 km long central transect starting at the breached levee and perpendicular to the river channel (A–A' in Fig. 3A). Complementary transects B–B' and C–C' were located approximately 1 km north (downstream) and south (upstream) from transect A–A', and were 1.85 and 1.40 km long, respectively. Transects D–D' and E–E' were located between three river-perpendicular transects. A hand-held GPS (Garmin International, Inc., Olathe, USA) was used to record the locations of the trenches and the sites at which we measured water depth and current direction. Using a shovel and a 30 cm long geoslicer (Takada et al., 2002), 59 trenches spaced ≈100 m apart were dug along the transects. The thicknesses, grain sizes, and sedimentary structures of the crevasse splay deposits were described at each trench. Water depth and current direction were measured using watermarks preserved on structures and the orientation of grass bent by the current, respectively. A global navigation satellite system receiver (ProMark 120; Ashtech, Santa Clara, USA) was used to measure the topographic profile along each transect, including the elevation of each trench and the watermarks.

3.1.2. Survey around the breached levee and estimation of pile thickness and volume

Field surveys around the breached levee were conducted over a period of five days between October 18 and November 26, 2019. The hand-held GPS was used to record the locations of the trenches and outcrops; trenches were dug at three locations at the south (upstream) gravelly pile along transect GP (GP-1–3) and nine locations at the north (downstream) sandy pile along transect SP (SP-1–9) (Fig. 5A and Table 1). The thickness, grain size, and sedimentary structures of the crevasse splay deposits were described at each trench and outcrop. At the gravelly pile, sediment samples were collected only at GP-3. We collected gravel samples at 20 cm^2 square over 10 cm vertical intervals at depths of 0–70 cm, and sand samples were collected over 2 cm vertical intervals at depths of 70–110 cm. In the sandy pile, trenches were dug using a shovel and the 30 cm long geoslicer. Samples taken by the geoslicer (at SP-3–9) were moved to another acrylic case at the field in order to return them to the laboratory. Sandy crevasse splay deposits were divided into 2 cm vertical intervals to conduct grain size and mud content analyses. No samples were collected at SP-1 and SP-2.

The thickness of the piles was estimated from the difference in elevation between the pile surface and pre-flood ground surface around the piles. The ProMark 120 was used to measure the elevation of the crevasse piles and pre-flood ground surface (Fig. 5B). We obtained the surface elevations of the piles by walking through them with the ProMark 120, which recorded the location, and elevation every second. Pre-flood surface elevations were measured based on the averages of thirteen points for the gravelly pile and two points for the sandy pile (Fig. 5B).

The areas of the piles were calculated using a software capable of analyzing particle size and shape in high-resolution photographs (Ishimura and Yamada, 2019). Then, the volumes of the piles were estimated from the calculated area, and the average thickness was obtained from the elevation survey.

3.2. Grain size analysis

In trenches along transects A–A', B–B', and C–C', sediment samples of several grams were collected for grain size analysis at 2 cm intervals from the top to the bottom of the sequence using a small spoon. Proximal splay deposits around the breached levee were sampled along transects GP and SP and the long-axis lengths of gravels at 0–70 cm depth in GP-3 were measured using a ruler.

Two approaches were used for grain size analysis. The grain sizes of the muddy samples from transects A–A', B–B', and C–C' were measured using a laser-diffraction particle size analyzer (LS 13 320; Beckman Coulter, Inc., Brea, USA) whereas those of the sandy and gravelly samples taken from transects GP and SP were measured using a Retch Technology CAMSIZER (Haan, Germany). The mud content of the proximal splay deposits at SP-3–9 were calculated based on the dry weight of the samples before and after mud removal. Organic matter was removed prior to the measurements using a 30% hydrogen peroxide solution applied for 24 hours.

Descriptive statistic values of the grain size distributions on the phi scale were calculated following the procedures of Folk and Ward (1957) and Folk (1966). Depth-averaged grain size distributions and mean grain sizes for each trench along the three river-perpendicular transects were then calculated by averaging the measurements.

3.3. Sedimentary structures

Sedimentary structures were described based on observations of the trenches or outcrops at survey sites. Furthermore, computed tomography (CT) images of samples at SP-3–9 were acquired using an Aquilion PRIME/Focus Edition (Canon Medical Systems Corporation, Tochigi, Japan) instrument at the Kochi Core Center, Japan. Sediment samples were imaged according to X-ray absorption such that high-density materials were identifiable by their relatively light colors (Falvard and Paris, 2017).

4. Geomorphological change and flood conditions

The 30 m wide and 5.0–5.5 m high levee revetment in the study site was fully breached over a distance of 70 m (Figs. 2, 5A, and 6A). Erosion was observed in the landside region around the breached levee up to 300 m upstream and 150 m downstream (Figs. 5A and 6C, D), whereas significant erosion was not observed in the riverside region (Investigation Committee on the Chikuma River Levee, 2020; Ohtsuka et al., 2021). Crevasse channels developed from the breached levee toward the floodplain and floodwater flowed mainly in three directions, influenced by the presence of artificial barricades, such as dwellings and a gymnastics hall (Figs. 5A, 6A, and 7A, B). These buildings were eventually destroyed by the floodwater (Figs. 6D and 7B). The channel eroded up to 3 m of pre-flood soil within 50 m of the breached levee (Investigation Committee on the Chikuma River Levee, 2020) such that only a 0.5 cm thick sandy deposit was present on the eroded surface at A-1 (34 m from the breached levee; Fig. 8A).

Sand and gravel sediment piles were observed at the outer side of the crevasse channel in aerial photographs acquired after the flooding (Figs. 2B, 5A, and 6A). Restoration work started immediately after the event and created the road and draining channel in the southern gravelly sediment pile (Figs. 5B and 7C), enabling observations of cross sections through the sediment pile at GP-1–3. On the other hand, the high-water channel on the river side of the levee was covered with muddy sediment, and cracks were observed only at the surface (Fig. 7D).

Along each transect, the measured elevation of the left bank levee revetment ranged from 338.0 to 338.5 m (Fig. 8A, C, and D). The height of the levee was approximately 5.0–5.5 m based on elevations determined immediately behind it, which ranged from 332.5 to 333.5 m. The elevation along each river-perpendicular transect descended at distances up to 1.1–1.4 km from the levee, such that the surface of the floodplain ascended at greater distances from the study area. The elevations of the lowermost areas in transects perpendicular to the river were approximately 330.5 m along transect A–A', 329.9 m along transect B–B', and 331.7 m along transect C–C', indicating that the elevation of the floodplain was lower in the northern downstream direction. Transect D–D' was almost flat, whereas the elevation of transect E–E' increased with distance from transect A–A' (Fig. 8B).

During the flooding event, flood currents spread out in a fan shape from the breached levee flowing toward the north–northwest around transects A–A' and B–B', and to the south–southwest around transect C–C' (Fig. 3B). The northward current predominated due to the gentle northward slope of the floodplain. Flood currents near the levee revetment flowed parallel to the levee.

The water depth, reconstructed from watermarks, was observed to correlate strongly with the elevation of the measured locations ($r = -0.76$; Fig. 9A) such that it increased from south to north: 0.6–2.0 m along transect C–C', 1.3–2.8 m along transect A–A', and 1.6–4.0 m along transect B–B' (Fig. 3A). This trend was attributed to the gentle northward slope of the floodplain. In contrast, water depths showed little change with distance from the levee in the studied transects (Figs. 8 and 9B), indicating that the river floodwater depth was only affected by elevation and not distance from the river.

5. Characteristics of crevasse splay deposits

The crevasse splay deposits studied herein were divided into three regions: proximal, medial, and distal splays based on the definition by Burns et al. (2017). The proximal splay was distributed around the breached levee, and was observed in transects GP and SP. The medial and distal splays were observed in transects A–A', B–B', C–C', D–D', and E–E'. Their characteristics are described in detail below.

5.1. Proximal crevasse splay deposits

5.1.1. Distribution and volume of sediment piles in the proximal splay deposits

Proximal crevasse splay deposits observed in the study area included gravelly or sandy sediment piles, and were distributed both to the south (upstream) and north (downstream) of the breached levee (Fig. 5A). The upstream gravelly pile was preserved on apple orchards and cultivated areas south of the breached levee and was estimated to cover an area of 6,630 m^2 according to image analysis. The downstream sandy pile was deposited in a park to the north of the breached levee and was estimated to cover an area of 4,340 m^2.

The volume of the upstream gravelly pile was estimated to be 8,020 m^3 based on its area and average thickness. The measured elevations of the gravelly pile ranged from 332.16 m (−0.23 m in thickness) to 334.73 m (2.34 m in thickness) whereas those of the pre-flood surface were 331.82–332.98 m (averaging 332.39 m; Fig. 5B). The average thickness of the gravelly pile inferred from elevation difference was 1.21 m when excluding results with negative thickness values. The Investigation Committee on the Chikuma River Levee (2020) estimated the volume of the gravelly pile to be 7,200 m^3, which is not significantly different from the results obtained herein. The measured elevation on the downstream sandy pile ranged from 331.86 m (−1.38 m) to 335.40 m (2.16 m) with an average thickness of 0.42 m calculated from the elevation of the pre-flood surface (averaging 333.24 m), similarly excluding results with negative thickness values. The volume of the downstream sandy pile was estimated to be 1,820 m^3.

5.1.2. Stratigraphy and sedimentary characteristics of sediment piles

The crevasse splay deposits in the gravelly pile consisted of lower sand layer (LSL) and upper gravel layer (UGL) bounded by a sharp interface (Figs. 10 and 11A). The interface between pre-flood soils and the lower sand layer was observed at GP-3, but could not be confirmed at localities GP-1 and GP-2 due to the high-water level in the artificial channel. Artificial materials and mud clasts were sometimes observed in the crevasse splay deposits, especially around the interface between lower sand and upper gravel layers. The thickness of the crevasse splay deposits ranged from 110 to 200 cm at GP-1–3, of which the lower sand layer accounted for 40–130 cm and the upper gravel layer for 70–130 cm (Fig. 11A). Although these data were obtained from only three sites, the average thickness of 150 cm did not differ significantly from that estimated from the elevation data (Fig. 5B). The thickness estimated from the elevation survey clearly decreased away from the breached levee (Fig. 5B).

The lower sand and upper gravel layers exhibited inverse and normal grading structures, respectively (Fig. 11). The crevasse splay deposit at 86–110 cm depth at GP-3 was mainly composed of medium to very coarse sand with rare gravels (Fig. 11B). In contrast, the gravel content increased, and the sand content decreased at 70–86 cm depth. In the upper gravel layer, at depths of 0–70 cm, the size of the gravels decreased toward the top (Fig. 11C). At GP-1 and GP-2, where a wide cross section could be observed, concave and trough cross-stratification was observed (Fig. 10A and B).

Crevasse splay deposits in the downstream sandy pile, the thickness of which ranged from 6.5 to 110 cm, exhibited various sedimentary facies (Figs. 12 and 13). At SP-1, SP-2, and SP-5, thicker gravelly deposits, and multiple inversely graded structures were observed. Cross-laminated sand layers were observed at SP-3, SP-4, and SP-8. An overlap of the finer sand layer and the mud cap at the surface was common to most sites studied herein (Figs. 13 and 14).

5.2. Characteristics of the medial and distal crevasse splay deposits

The medial crevasse splay deposits distributed within 800 m of the breached levee were composed of lower sandy (muddy sand or sandy mud) layers and the upper mud layers (Fig. 8A). These deposits were observed along transects A–A' (A-2–6), D–D', and E–E' (Fig. 15A and B); they were relatively thicker along transect E–E' (south and upstream) than at transect D–D' (north and downstream) (Fig. 8B). The thickness of the sandy layer of the medial crevasse splay deposit decreased with distance from the breached levee (Figs. 8A, B, and 9D).

At distance from the levee, distal crevasse splay deposits composed of massive mud were observed at A-7–13 along the central transect A–A' (Figs. 8A and 15C). These distal deposits were also observed along transects B–B' and C–C' 1 km north and south of the central transect A–A' (Figs. 8C, D, and 15D). The deposits were not observed to thin away from the levee in either transect (Figs. 8 and 9C, D) and no deposit was observed near the limit of the inundation area along transects A–A' and B–B' (Fig. 8A and C).

Regarding grain size distribution, both the medial and distal crevasse splay deposits were observed to fine away from the levee (Figs. 8 and 16). The medial crevasse splay deposit was mainly composed of upward-fining very fine sand and silt (3–5 phi; Fig. 17). The top of the medial and distal crevasse splay deposits mainly consisted of silt (4–8 phi) and were finer than the lower deposits.

The maximum extents of the sandy (medial splay) and muddy (distal splay) deposits differed significantly as a function of inundation distance. Along the 2.23 km long central transect A–A', these layers of the medial splay extended up to 0.80 km away from the levee, whereas the mud layer of the distal splay prevailed up to a distance of 1.60 km (Fig. 8A). Their maximum extents were 35.7% and 71.8% of the inundation distance (2.23 km), respectively. Along the 1.85 km long transect B–B' and the 1.40 km long transect C–C', the mud layer was present up to 1.51 and 1.35 km away from the levee, respectively (Fig. 8C and D). The maximum limits of the mud layer of the distal splay were 81.7% and 70.8% of the inundation distances of transects B–B' (1.85 km) and C–C' (1.91 km), respectively. The ratio of the extent of the sand layer of the medial splay to that of the mud layer of the distal splay was 49.7% along transect A–A', the only transect in which the sandy layer was observed.

6. Discussion

6.1. Influences on the distribution of the crevasse splay deposits

Field surveys revealed that the sandy layer in the medial crevasse splay deposits varied as a function of distance from the breached levee. In contrast, the muddy layer of the distal splay is distributed as a function of the elevation of the floodplain in addition to the distance (Figs. 8 and 9C, D). The inundation water depth was almost constant irrespective of distance from the levee (Fig. 9B). The thickness of the sandy layer in the medial crevasse splay deposit decreased with distance, indicating that water depth was not a deterministic factor for the deposition of sandy sediment. The sandy layer was observed to have an inland-thinning trend, probably due to rapid deceleration of the flood flow, implying that the bedload played a primary role in transporting sandy sediments. The flow velocity would have rapidly decreased when the flood flow reached the wider floodplain through the breached levee. As such, it can be expected that artificial barricades, including dwellings, and the gymnastic hall near the breached levee (Fig. 5A), also reduced the flow velocity such that the flood flows were unable to transport sand grains significant distances from the breached levee (< 800 m).

In contrast, the muddy layer of the medial and distal crevasse splay deposits became thicker as the elevation decreased, in addition to the distance from the breached levee (Figs. 8 and 9C, D). The strong negative correlation between elevation and inundation water depth indicates that the water depth influenced the thickness of the mud layer, implying that muddy sediments settled from a suspended load in stagnant water. The upward-fining trend of the muddy layer also suggests suspension fallout from the water column (Fig. 17).

6.2. Importance of the maximum extent of crevasse splay deposits for evaluating past river flooding events

The maximum extents of the medial and distal crevasse splay deposits were 0–35.7% and 70.8–81.7% of the inundation distance, respectively. The distal crevasse splay deposits composed of muddy sediment dominated the entirety of the inundation area. Therefore, identifying the distribution of muddy deposits is necessary for reconstructing the inundation area of past river flood events.

Observed trends in the extent of sandy (proximal and medial) and muddy (distal) crevasse splay deposits in the study area show good agreement with those reported in previous studies on modern crevasse splay deposits (Smith et al., 1989; Farrell, 2001; Fisher et al., 2008; Arnaud-Fassetta, 2013; Matsumoto et al., 2016; Toonen et al., 2016; Sato et al., 2017; Rahman et al., 2022a). Matsumoto et al. (2016) determined the limits of the inundation area (2.90 km) and sandy deposits (0.62 km) from a levee breached by the September 2015 flooding of the Kinu River, Central Japan. Sato et al. (2017) also investigated flood deposits caused by this flooding event, showing that a change from sandy to muddy deposits occurred approximately 0.6–0.7 km from the breached levee. The maximum extent of the sandy crevasse splay deposit was calculated to be 21.4% of the inundation distance, implying that the sandy sediment was deposited within a limited distance of the flood inundation. Arnaud-Fassetta (2013) investigated sedimentary sequences of single crevasse splays at two localities caused by the 2003 flooding in the Rhône Delta, France, finding that the sandy and sandy silt proximal splays are distributed only up to 1570 m from the breached levee, whereas muddy distal splays are distributed up to 20 km. Rahman et al. (2022a) identified a single crevasse splay in Google Earth imagery along the Magdalena River, Colombia. Although the extent of inundation is unknown, they confirmed that distal splay is distributed about twice as far as proximal–medial splays.

A similar trend has been observed in ancient crevasse splay deposits. Burns et al. (2017) investigated ancient crevasse splay deposits at 35 locations in the Cretaceous Castlegate Sandstone and Nelson Formation of the Mesaverde Group, eastern Utah, USA, finding that these deposits exhibit thinning and fining trends with distance from their source river. In the proximal parts of splays near the river (129 m in mean lateral extent from a crevasse channel), the deposits include cross-laminated sandstones, but they thin and fine gradationally into the medial and distal parts of splays far from the river (333 m and 562 m in mean lateral extent, respectively); our own observations are consistent with this model.

The ratio of the extent of the sandy layer (medial splay) to that of the muddy layer (distal splay) in this study was 49.7% and could be an important metric for determining the scale of a levee breach. The mean lateral extents of proximal and medial splays relative to distal splay are 23.0% and 59.3%, respectively (Burns et al., 2017). Since it is difficult to accurately reconstruct the inundation distance of past river floods from geological records, differences in the ratio between sandy and muddy deposits can facilitate evaluation of the magnitude of past river floodings. Although this is difficult to examine due to the lack of other modern single crevasse splay studies that consider the distributions of both muddy and sandy crevasse splay deposits, this ratio may nonetheless be an indicator for the scale of a levee breach when the size and morphology of the crevasse splay deposit can be observed to change with the size of the breach.

6.3. Source of sediment piles (crevasse splay deposits)

The sediment piles of the proximal splay deposit at the breached levee likely represent a redeposition of the interior components of the breached levee. The volume of these sediment piles is less than the amount of levee erosion; the volumes of the upstream gravelly pile and downstream sandy pile were estimated to be 8,020 m^3 and 4,340 m^3, respectively. Considering that the total volume of released sediments was estimated to be 20,560 m^3 (Investigation Committee on the Chikuma River Levee, 2020), the internal components of the levee alone are sufficient to account for the volumes of both sediment piles. Additionally, only mud was deposited on the river side of the levee (Fig. 7D). If the large amounts of gravel and coarser sand particles in the sediment piles we sourced from the river, they would also be expected to be deposited on the river side of the levee; however, since only thick muddy deposits were observed in that location, gravel, and coarser sand particles are unlikely to have been supplied by the river. Thus, gravel and coarser sand particles transported as bedload through the low water channel were not brought to the higher elevation high-water channel (Fig. 2C). Furthermore, gravelly material has rarely been identified in both modern and ancient crevasse splay deposits (e.g., Bristow et al., 1999; Arnaud-Fassetta, 2013; Matsumoto et al., 2016; Burns et al., 2017; Widera et al., 2023) because natural levees comprise sandy sediments, and the crevasse splay deposits formed by their breach are also sandy. Actually, in the 2015 flooding of the Kinu River, where sandy crevasse splay deposits were observed (Matsumoto et al., 2016; Sato et al., 2017), the interior of the breached levee was composed of sandy sediments (Investigation Committee on the Kinu River Levee, 2016).

It is thus concluded that the gravelly sediment piles formed were rare as crevasse splay deposits. Hori and Hirouchi (2011) also reported gravelly crevasse splay deposits caused by the 2004 flooding of the Asuwa River, Central Japan. They have not confirmed the internal structure of the levee revetment, but they infer that gravelly sediments were likely used in the levee and supplied during the flooding event. Although gravelly crevasse splay deposits such as those studied herein have not been observed in natural rivers, where most known crevasse splays have been studied (e.g., Smith et al., 1989; Farrell, 2001), such deposits may form at more sites in the future, especially in artificially embanked rivers.

6.4. Levee breaching and sedimentation processes

In the example studied herein, features of crevasse splay deposits strongly reflect the internal structure of the breached levee; therefore, the process of levee breaching can be expected to be inferred from the crevasse splay deposits. By virtue of the CCTV camera installed on the breached levee, a time series record of the overflow and levee breaching processes is available (Figs. 2, 4, and 18A).

The following subsections describe levee breaching and sedimentation processes in four stages (Fig. 18) which are correlated to the formation of the crevasse splay deposit. The sedimentary facies of the downstream sandy piles are found to be more complex than those of the upstream gravelly pile due to the influence of obstacles, such as the gymnastic hall and houses (Figs. 5A and 6A). Thus, the reconstruction of the levee breaching process is mainly based on the sedimentary facies of the upstream gravelly pile.

6.4.1. Overflow stage

The video recorded by the CCTV camera installed on the breached levee revealed that river water overflow occurred at 0:55 am (Fig. 4; Investigation Committee on the Chikuma River Levee, 2020). The camera collapsed at the end of the 2:15 am video;

thus, the overflow continued for at least 80 minutes. It is presumed that the landside caused by erosion of the levee also began during this time (Figs. 5A, 6C, D, and 18A). Of the factors contributing to the levee breach, external (landside) erosion due to overflowing has been found to be the most frequent (Özer et al., 2020).

During the overflow stage, mud and finer sand particles transported in suspension from upstream would have been brought to the floodplain (Fig. 18A); however, most of these particles were likely eroded during the subsequent levee breach stages. Fine-grained sediment transported in the suspended load of the overflowing current cannot be observed in the lowest part of the gravelly pile, which is instead composed of coarser sand sourced from the levee (Figs. 10 and 11). The lowest part of the sandy pile exhibits low mud content (Fig. 14); thus, all sediment in the piles was deposited during the later levee breaching stage.

6.4.2. Early stage of levee breach (partial breach)

The levee breach is estimated to have occurred around 2:15 am (Fig. 4; Investigation Committee on the Chikuma River Levee, 2020), although the total time of the breach is not known. Given that the levee was confirmed to have fully breached at 5:00 am, the breaching may have lasted for almost three hours. According to the report of the breached levee investigation, the levee breach is attributed to external erosion by overflow and structural weakness of the levee revetment, and it is assumed that the levee breach started from the downstream side of the levee (Investigation Committee on the Chikuma River Levee, 2020; Ohtsuka et al., 2021).

The upstream gravelly pile is characterized by lower sand and upper gravel layers with a clear boundary (Fig. 10), implying that the levee breach can be divided into two phases. As noted above, macroscopic changes in the thickness of the sand layer indicate that the lower layer did not form during the overflow stage but during this early breaching stage. The presence of destroyed artificial materials in the sand layer at GP-1 further supports this (Fig. 10A). The presence of sandy soil on the outer side of the levee revetment structure suggests the eroded sand particles were transported during this stage (Figs. 6B and 18B). In the lower sand layer at GP-3, the content rate of granules is larger above 86 cm depth (Fig. 11B), suggesting either that the flow strength increased around this depth, allowing coarser-grained granules to reach this area, or that bank erosion partly reached the inner gravel layer and began to supply granules. Lateral changes in the grain size distribution of the lower sand layer could have been used to resolve this, but the limited number of locations at which such deposits could be observed renders it impossible to determine which was the primary factor.

The majority of the downstream sandy pile is sand particles (Fig. 13), suggesting that it formed during this stage. This is supported by the fact that the levee breach began at the downstream side of the levee, which is composed of sandy soil (Investigation Committee on the Chikuma River Levee, 2020; Ohtsuka et al., 2021).

6.4.3. Later stage of levee breach (full breach)

During this stage, river water began to erode the gravelly soil in the central and upstream parts of the levee revetment such that the majority of material supplied to the floodplain was of gravel grade (Figs. 6A and 18C). The upper gravel layer in GP-3 shows clear grading (Fig. 11A and C), suggesting a gradual decrease in the flow shear stress causing fining of gravel size. Thus, the flow strength was at its maximum when the gravel layer began to deposit, then, and gradually weakened toward the top of the sequence. The presence of artificial materials and large mud clasts near the boundary between the lower sand and upper gravel layers also indicates a peak in flow strength during this phase (Figs. 10 and 11).

Since gravels were also common in SP-1 and SP-2 at the downstream sediment pile, it is assumed to have been deposited during this stage, when active flooding flow discharged from the breached levee. They exhibited several three inverse grading layers, implying that the flow intensity fluctuated at least three times. These velocity fluctuations may correspond to small-scale avulsions during this stage.

6.4.4. Stagnant stage

During the stagnant stage, sandy and gravelly sediments had already settled out of the flooding flow, and mud was depositing primarily in the lower elevation regions of the inundation area (Fig. 18D). Here, the stagnant stage refers to the period after the cessation of the flood flow, when the entire floodplain was submerged. Since the water level at the upstream Kuiseke gauging station began to reduce before the levee breach whereas that at the downstream Tategahana gauging station reduced after the breach (Fig. 4), it is presumed that the water level in the study site began to lower soon after the levee breach. No mud layers were observed on the surface of the upstream gravelly pile (Figs. 7A, 10, and 11), suggesting that the stagnant water level was below the surface of the gravelly pile. The finer sand layer and mud cap observed at the surface of the downstream sandy pile were probably deposited during this stage (Figs. 12–14). The absence of deposits near the inundation limit implies that the stagnant water stood for only a short period of time in this area before receding, since the elevation of this area is higher than that at which the thick mud was observed (Fig. 8).

7. Conclusion

This study investigated three regions of crevasse splay deposits (proximal, medial, and distal splays) caused by the October 2019 flooding event of the Chikuma River in Central Japan. The levee breaching process was reconstructed based on the sedimentary characteristics of the sediment piles (proximal splay) formed behind the breached levee based on comparisons with the internal structure of the levee. In addition, sedimentological and hydraulic investigations covering the entire inundation area immediately after flooding revealed the wide-scale distribution characteristics of the crevasse splay deposits (medial and distal splays) and the hydraulic factors that contribute to their distribution. The data and findings in this study should be useful for similar facies analysis of ancient crevasse splay deposits.

The proximal splay (sediment pile) was distributed around the breached levee. The upstream gravelly sediment pile was characterized by lower sandy and upper gravelly layers bounded by a sharp contact. These sedimentary facies reflect a levee breaching process in which the outer sandy soil of the artificial levee began to be scoured by external erosion, after which the erosion of the inner gravelly soil occurred. During the following stagnant stage, little sand and gravel deposition would have occurred, and mud would have been deposited at lower elevations within the inundation area. Within the study area, a gravelly crevasse splay deposit, unknown from previous studies of similar sequences, was observed, which was attributed to the internal structure of the artificial levee revetment. This study suggests that the sedimentary characteristics of proximal splay deposits are strongly controlled by the local environment but are nonetheless useful for inverse analysis of progressive process in both past and future levee breach events.

Outside the proximal splay, sandy crevasse splay deposits (the medial splay) was distributed within 800 m of the breached levee within a total inundation distance of 2.23

km, thinning away from the breached levee. In contrast, muddy crevasse splay deposits (the distal splay) were relatively thick in topographic lows where higher water depths were recorded, but did not correlate with the distance from the river. These results imply that sand deposition was influenced by distance from the breached levee and that the deposition of mud was affected by water depth in addition to the distance from the breached levee. The maximum limit of sandy deposits (the medial splay) was 35.7% of the inundation distance, whereas muddy deposits (the distal splay) extended to 70.8–81.7% of the total inundation distance. This suggests that it is important to determine the extent of muddy crevasse splay deposits (distal splay) from the geologic strata to determine the total inundation area of past levee breaches.

Acknowledgments

This study was partly supported by a research grant from the Institute of Mountain Science, Shinshu University (T. Tokiwa) and a research grant from the Kyoto University Foundation (H. Naruse). The CT image scanning was performed under the cooperative research program of the Center for Advanced Marine Core Research, Kochi University (Accept No. 20B052). Most of the figures were generated by Generic Mapping Tools (Wessel et al., 2019). The authors would like to thank Enago (www.enago.jp) for the English language review.

Table 1. Location and thickness of crevasse splay deposits at each trench and outcrop sampled or observed.

Trench / Outcrop	Latitude	Longitude	Distance from the breached levee (m)	Thickness (cm)
Gravelly pile				
GP-1	36.685651	138.274150	115	>200
GP-2	36.685658	138.273958	131	>180
GP-3	36.685591	138.273584	166	110
Sandy pile				
SP-1	36.686652	138.275906	99	ca. 110
SP-2	36.686715	138.275928	106	ca. 100
SP-3	36.686719	138.275946	107	39
SP-4	36.686759	138.275954	111	20
SP-5	36.686850	138.275850	118	36–39
SP-6	36.686818	138.275966	118	6.5
SP-7	36.686863	138.275985	123	8.5
SP-8	36.686918	138.276026	130	35
SP-9	36.686949	138.275995	133	14

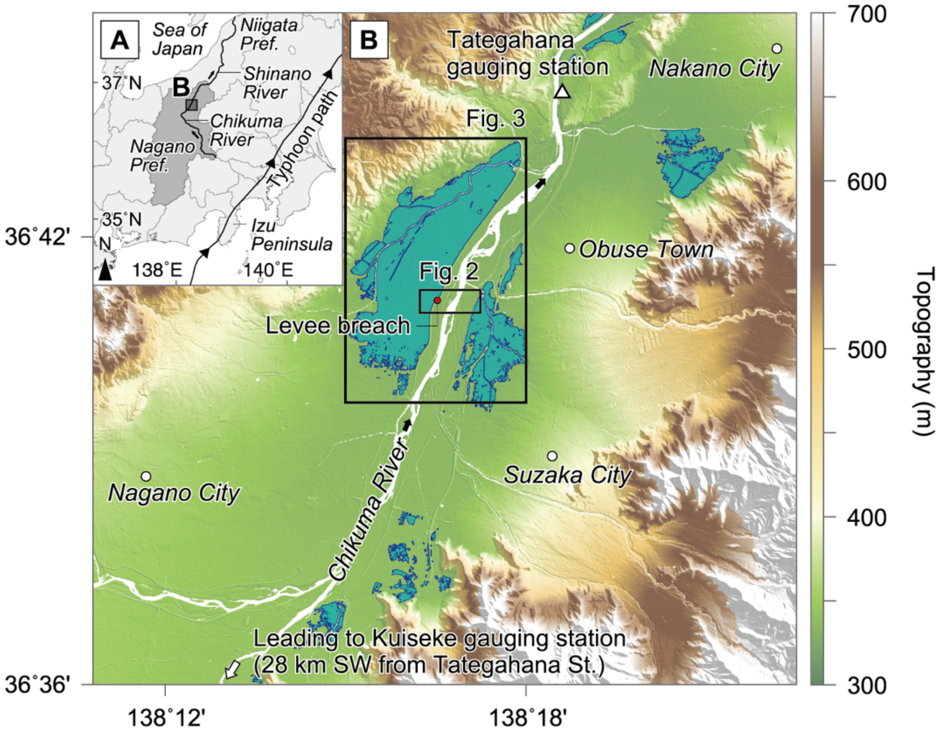

Fig. 1. Location map of the study area. (A) Location of the Chikuma River (Nagano Prefecture)/Shinano River (Niigata Prefecture), Central Japan. The path of the typhoon is also shown (Japan Meteorological Agency, 2019). (B) Digital elevation model showing the study area around the Chikuma River (Geospatial Information Authority of Japan, 2015). The extent of the October 2019 flooding, estimated from aerial photographs taken immediately after the event by the Geospatial Information Authority of Japan (2019), is also shown.

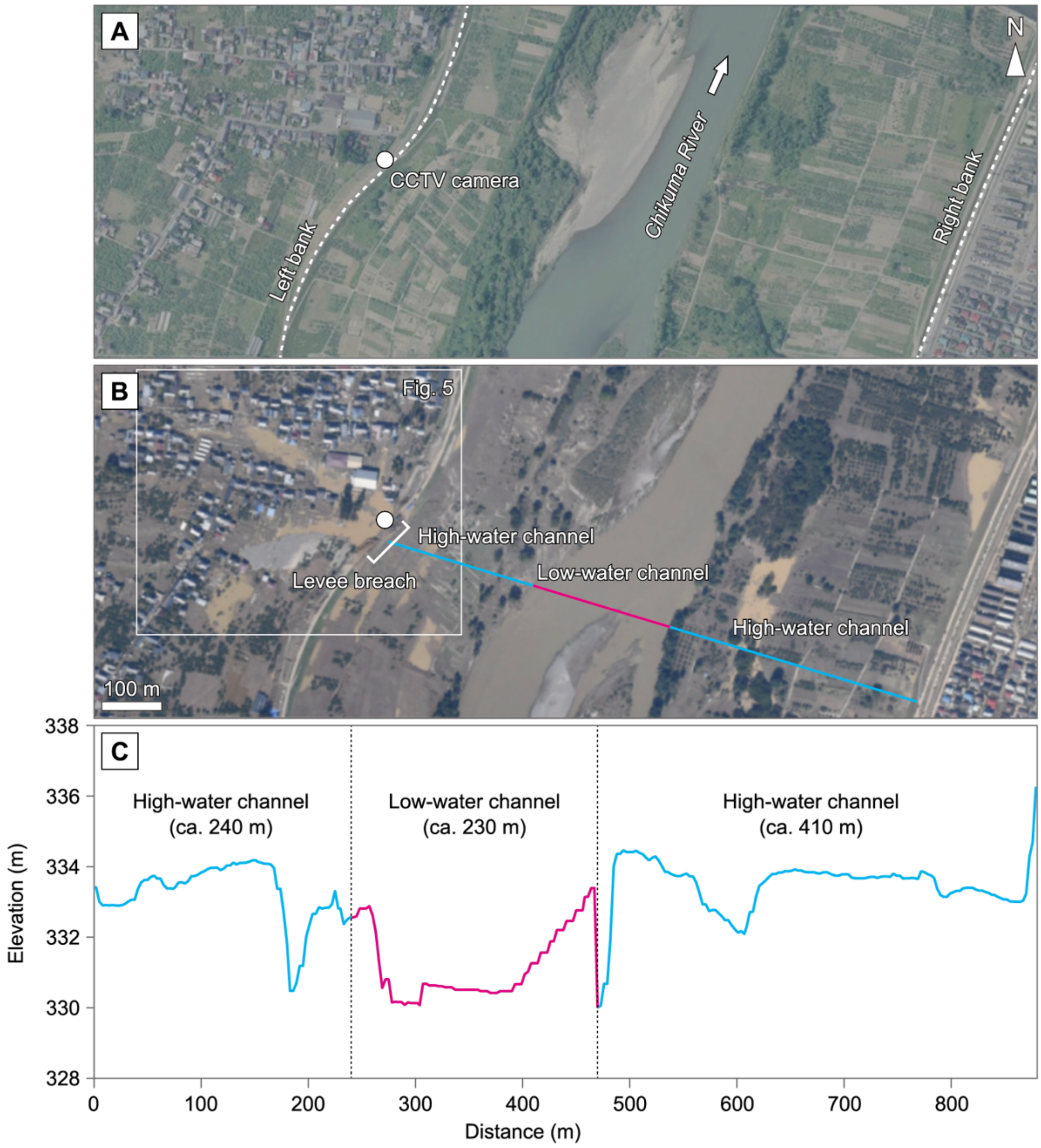

Fig. 2. Aerial photographs around the study site. (A) Before the flooding (photograph taken in 2010). (B) After the flooding (photograph taken on October 16, 2019) (Geospatial Information Authority of Japan, 2019). Locations of low-water (pink line) and high-water (blue line) channels, CCTV camera, and the levee breach are shown. (C) Channel cross-section and width during low water and high water stages (created from DEM data provided by the Geospatial Information Authority of Japan).

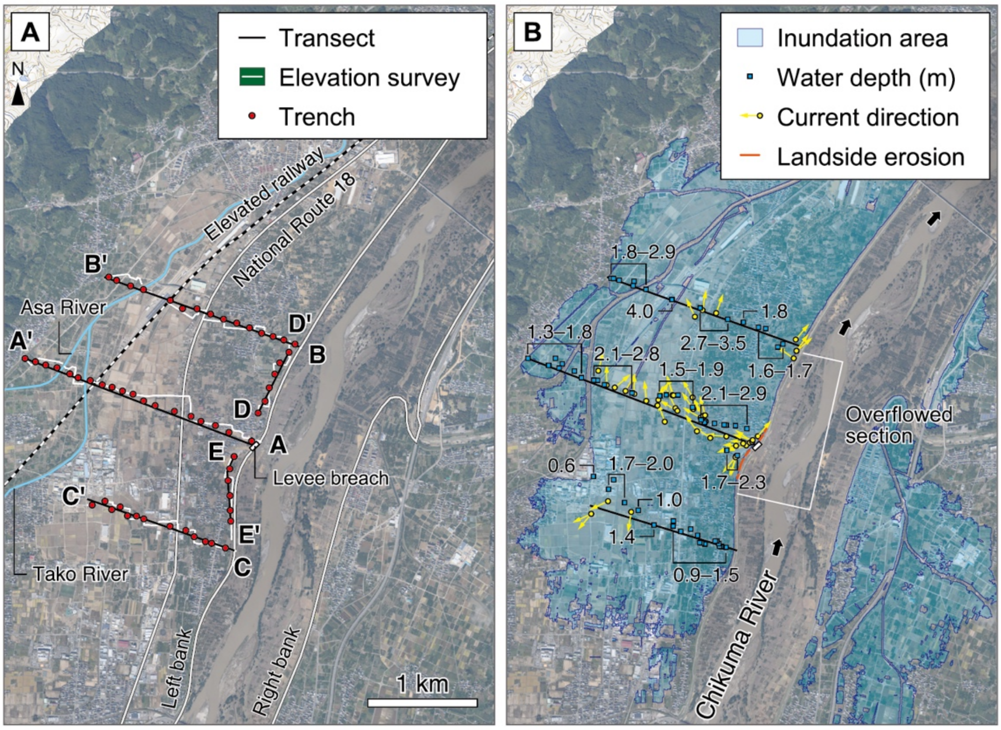

Fig. 3. (A) Locations of the breached levee, transects A–A' to E–E', trenches, and the route of the elevation survey (white line). (B) Measured water depth and current direction of flooding along and around the transects. Aerial photograph of the study site after the flooding was provided by the Geospatial Information Authority of Japan (2019).

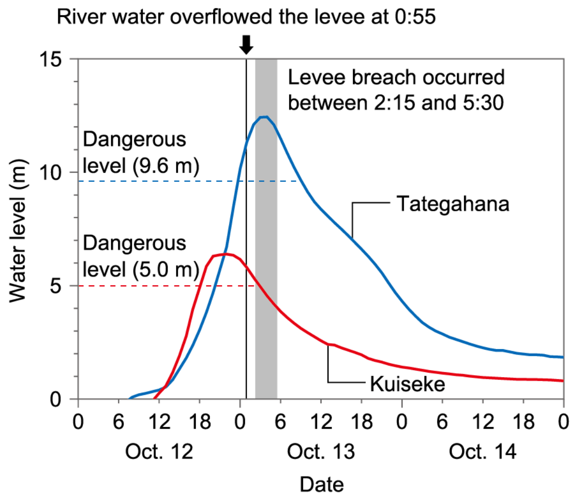

Fig. 4. Water level change from October 12 to October 14 recorded at the Kuiseke (upstream) and Tategahana (downstream) gouging stations (see Fig. 1 for locations). Dangerous water levels for river flooding at each gauging station set by the Chikuma River Office are also shown. Overflowing and breaching of the levee at the study site are assumed to have occurred 0:55 am and 2:15–5:30 am, October 13, respectively (Investigation Committee on the Chikuma River Levee, 2020).

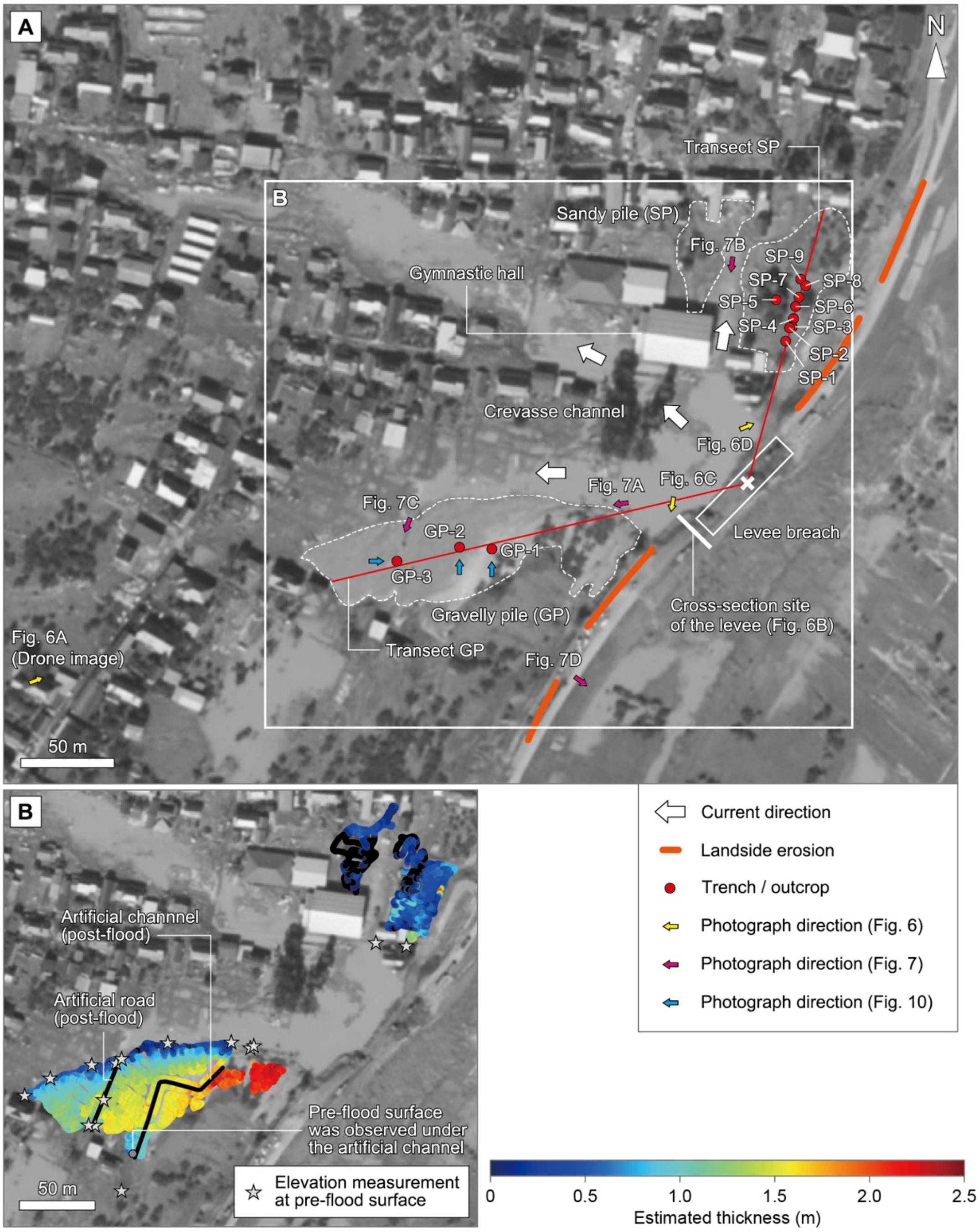

Fig. 5. (A) Aerial photograph around the breached levee (Geospatial Information Authority of Japan, 2019), showing the locations of the gravelly pile (GP), sandy pile (SP), transects GP and SP, and the surveyed trenches and outcrops. Yellow, pink, and blue arrows represent photograph directions in Figs. 6, 7, and 10, respectively. (B) Estimated thickness of the gravelly and sandy piles. Pre-flood surface elevation was measured at the points indicated with stars.

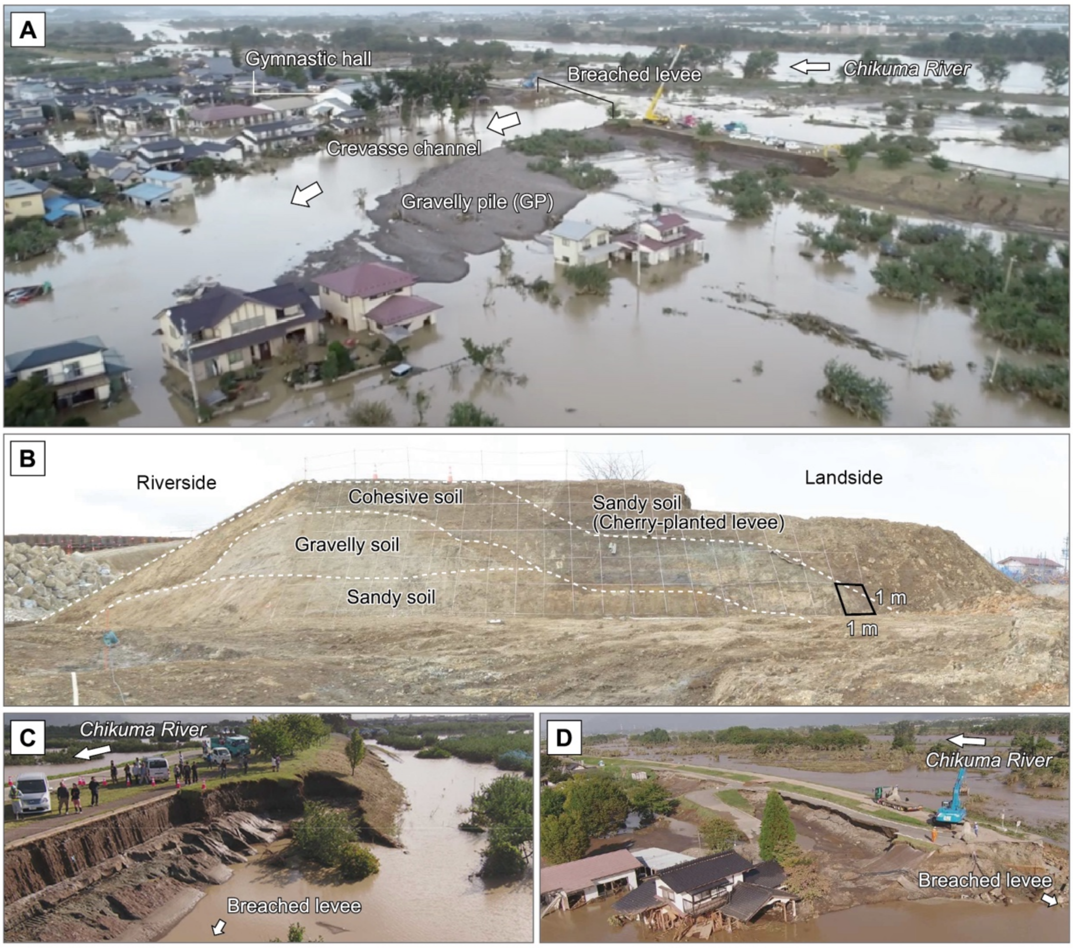

Fig. 6. (A) Drone image taken at approximately 5 pm on October 13 by the Geospatial Information Authority of Japan. (B) Upstream cross section of the breached levee. (C) Photograph of the upstream side of the breached levee. (D) Photograph of the downstream side of the breached levee. Photograph locations and directions are indicated in Fig. 5. Photographs were taken on (B) February 8, 2020, and (C and D) October 13, 2019, by the Investigation Committee on the Chikuma River Levee (2020).

Fig. 7. Photographs of (A) crevasse channel and gravelly pile (proximal splay), (B) crevasse channel and sandy pile (proximal splay), (C) artificial road in the gravelly pile (proximal splay) created after the flooding, and (D) muddy deposit preserved in the high-water channel. Photograph locations and directions are indicated in Fig. 5.

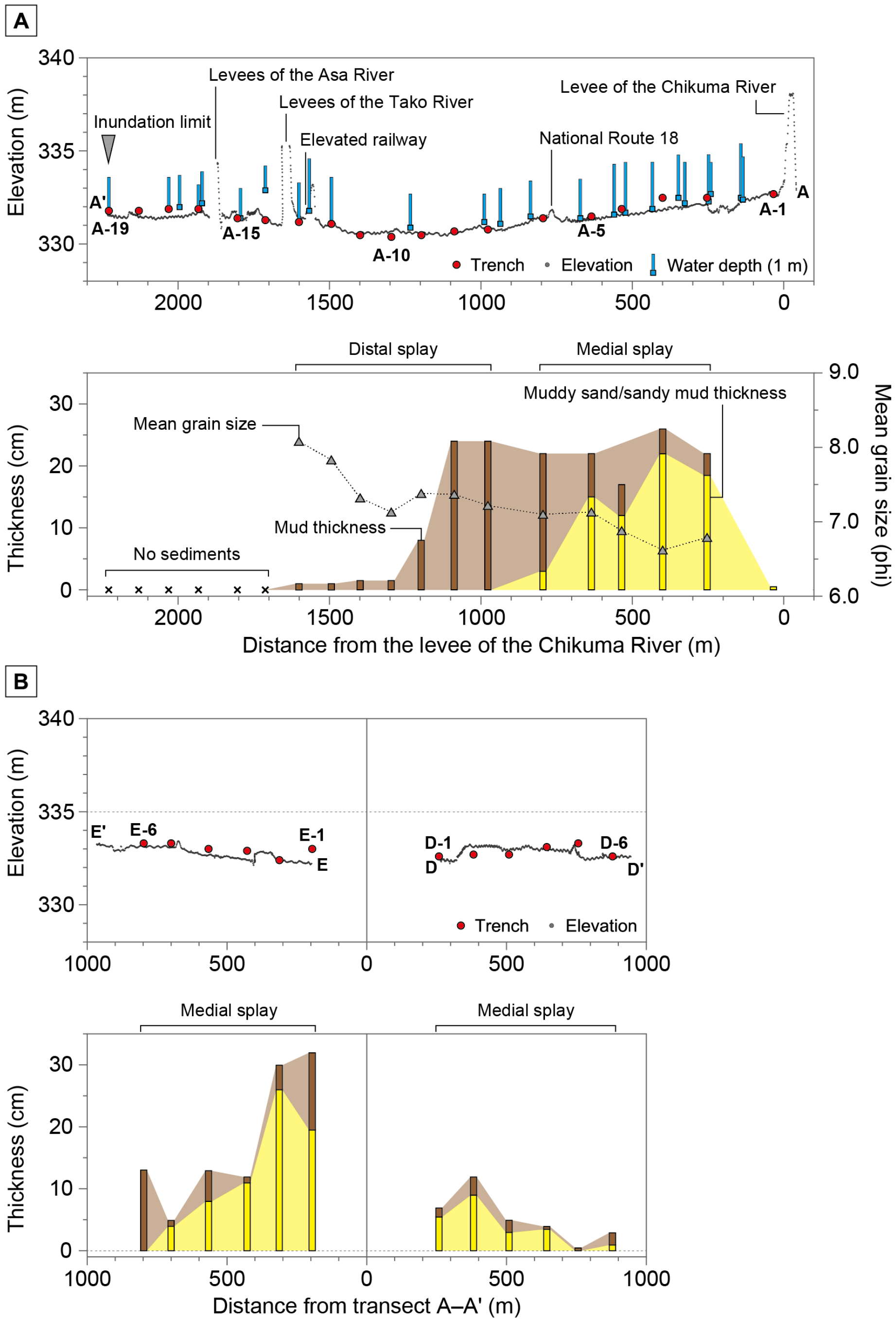

Fig. 8. Measured elevation, water depth, and thickness, and mean grain size of crevasse splay deposits. (A) transect A–A' with trench locations (A-1 to A-19), (B) transects D–D' and E–E' with trench locations (D-1 to D-6 and E-1 to E-6), (C) transect B–B' with trench locations (B-1 to B-15), and (D) transect C–C' with trench locations (C-1 to C-13).

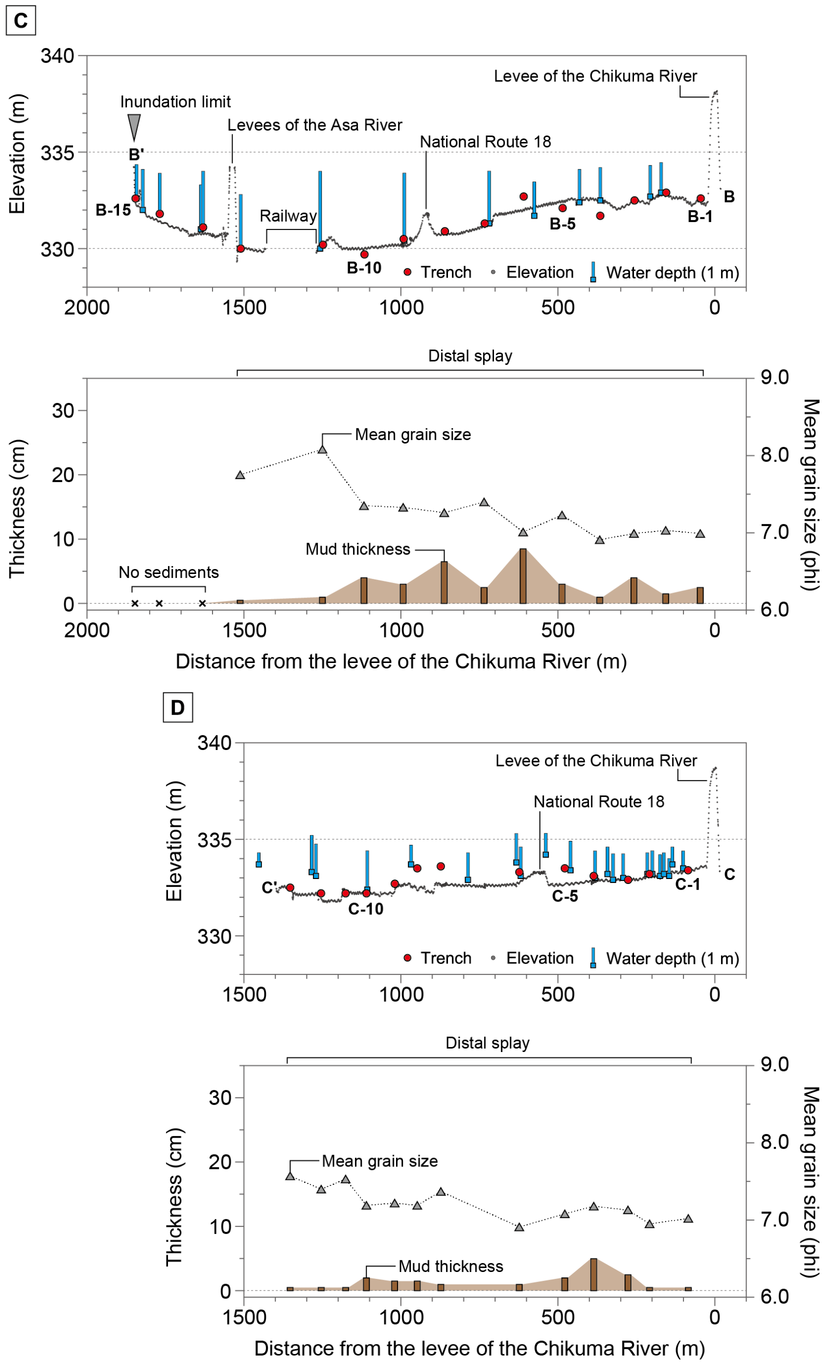

669

670 **Fig. 8.** *(continued)*.

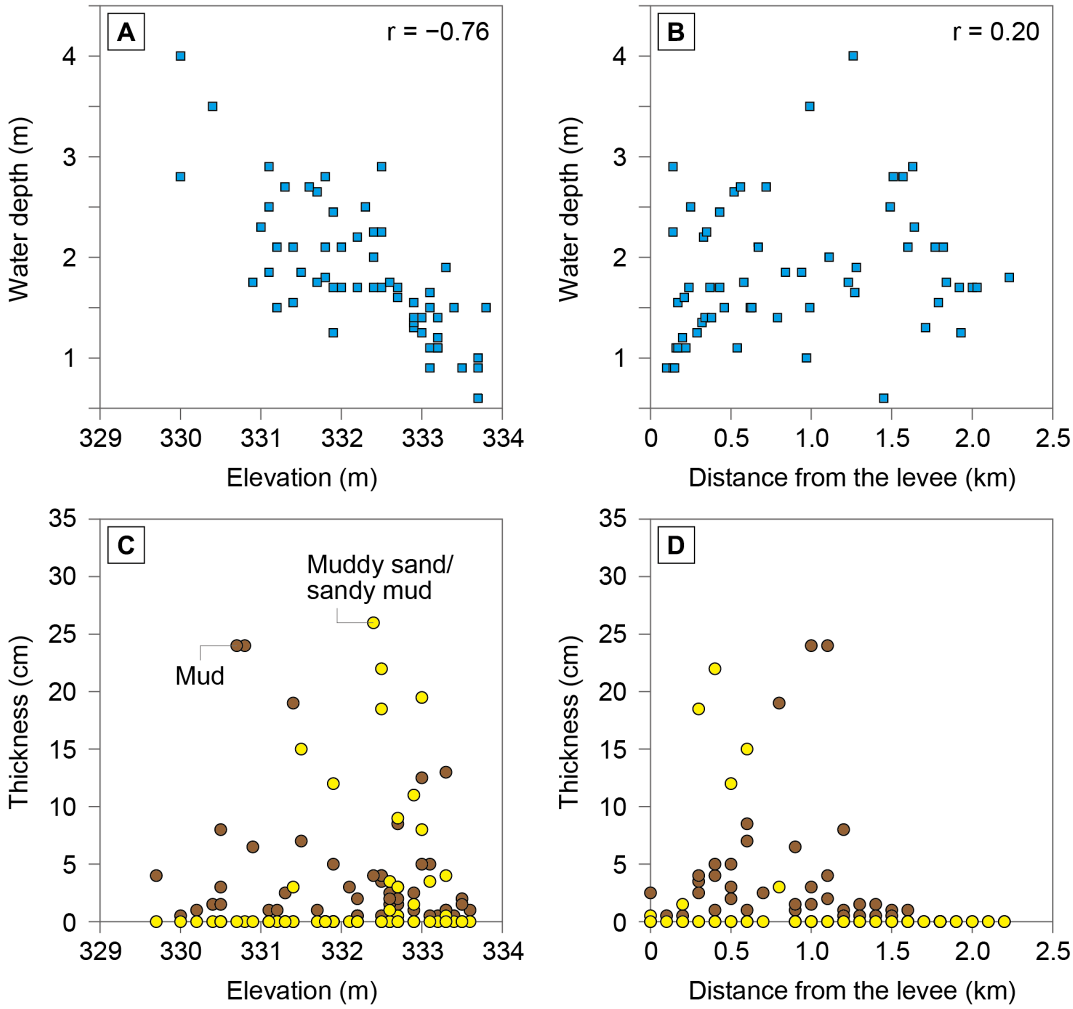

Fig. 9. Comparison between water depth and deposit thickness with elevation and distance from the levee. Relationships between (A) water depth and elevation, (B) water depth and distance from the levee, (C) thickness and elevation, and (D) thickness and distance from the levee. Note that (C) shows all data, including transects D–D' and E–E', whereas (D) shows data only for the river-perpendicular transects A–A', B–B', and C–C'.

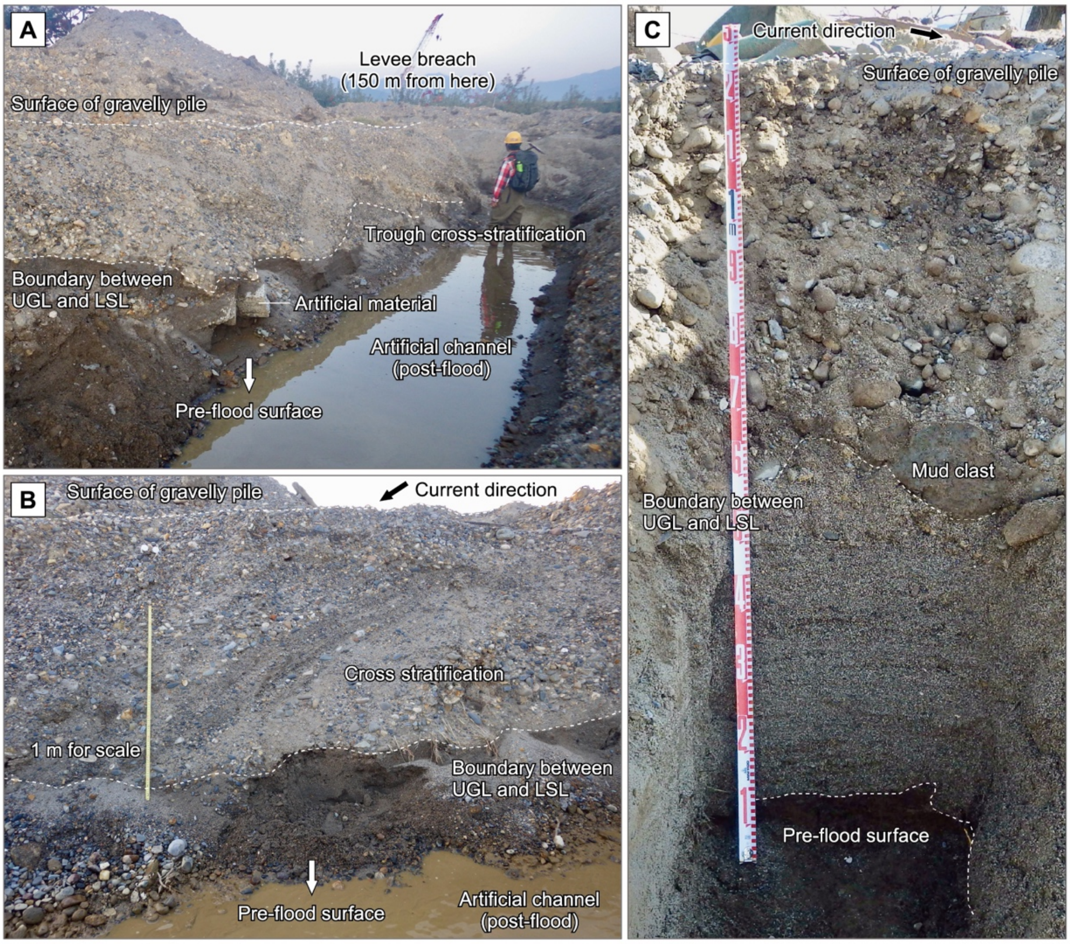

Fig. 10. Photographs showing crevasse splay deposits at (A) GP-1, (B) GP-2, and (C) GP-3 in the gravelly pile (proximal splay). Photograph locations and directions are indicated in Fig. 5.

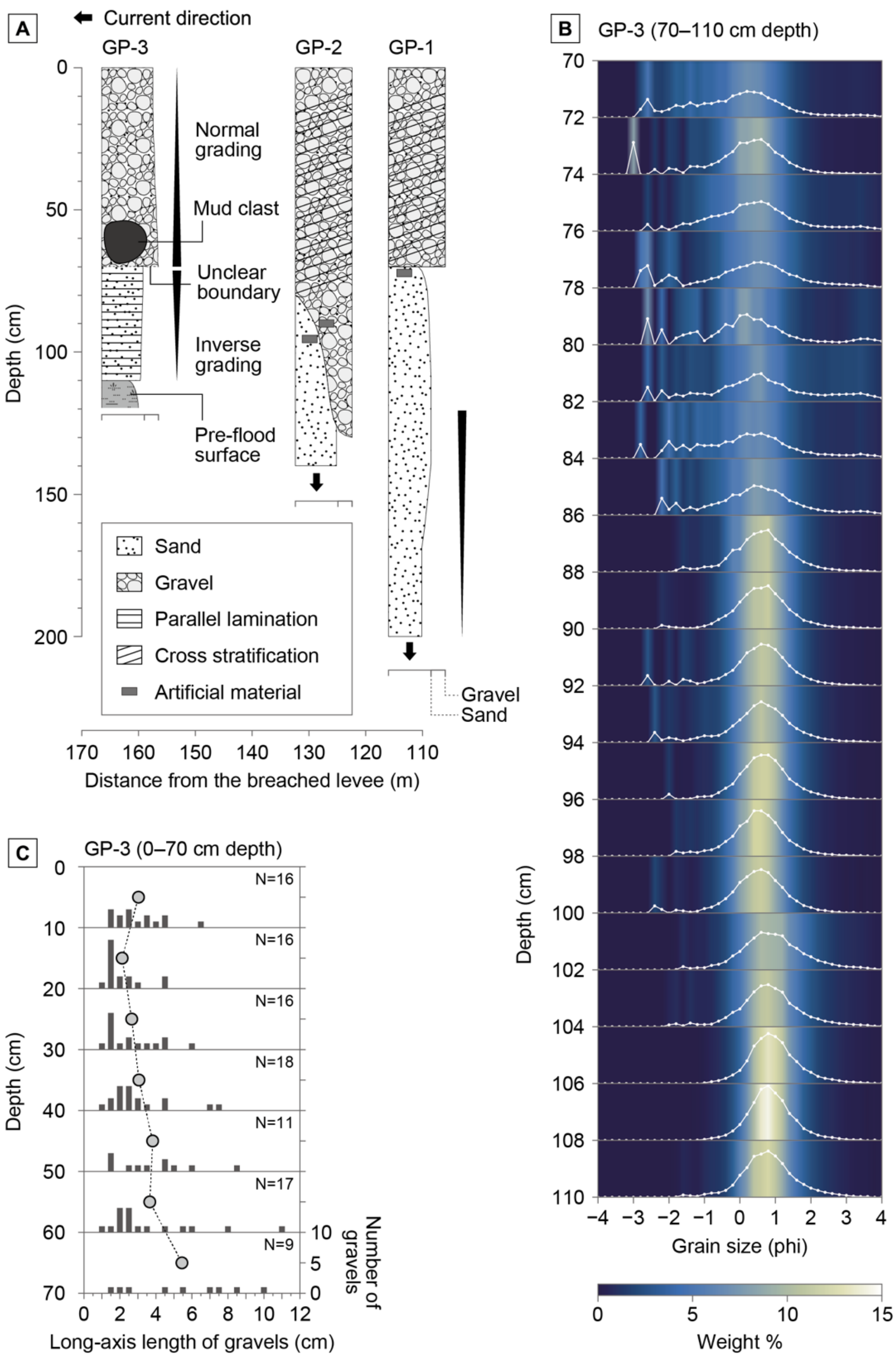

Fig. 11. (A) Columnar section of crevasse splay deposits at GP-1–3 in the upstream gravelly pile (proximal splay). (B) Vertical change in grain size distribution of the crevasse splays deposit at 70–110 cm depth at GP-3. (C) Distribution and average (gray circle) long-axis length of gravels in the crevasse splay deposit at 0–70 cm depth at GP-3.

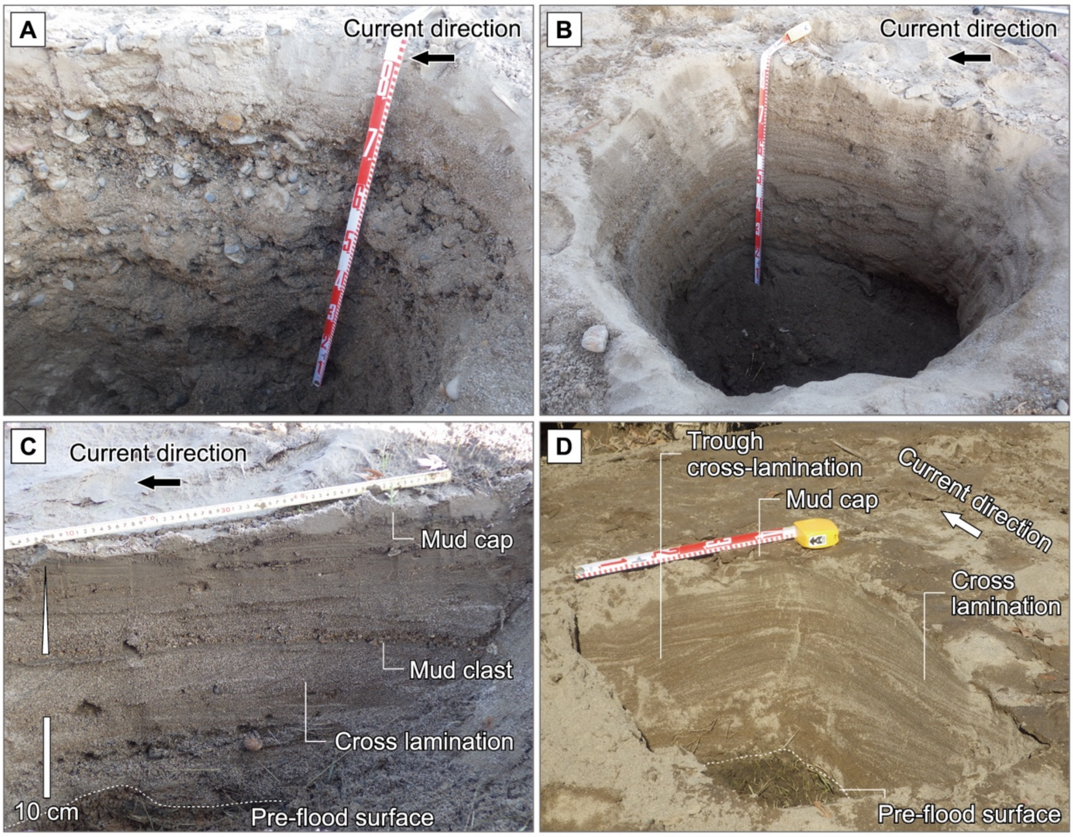

Fig. 12. Photographs showing crevasse splay deposits at (A) SP-1, (B) SP-2, (C) SP-3, and (D) SP-8 in the sandy pile (proximal splay).

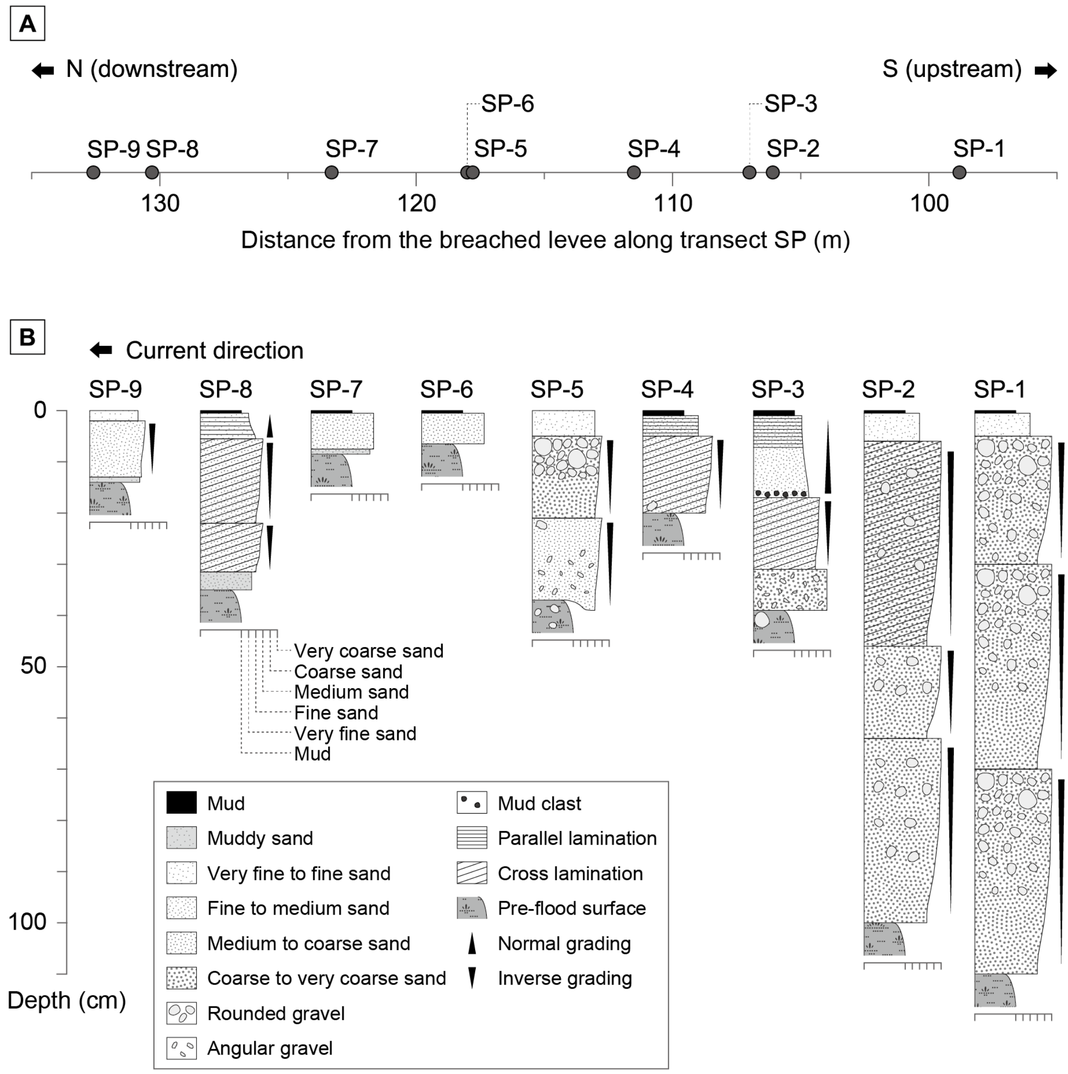

Fig. 13. Columnar section of crevasse splay deposits in the downstream sandy pile (proximal splay).

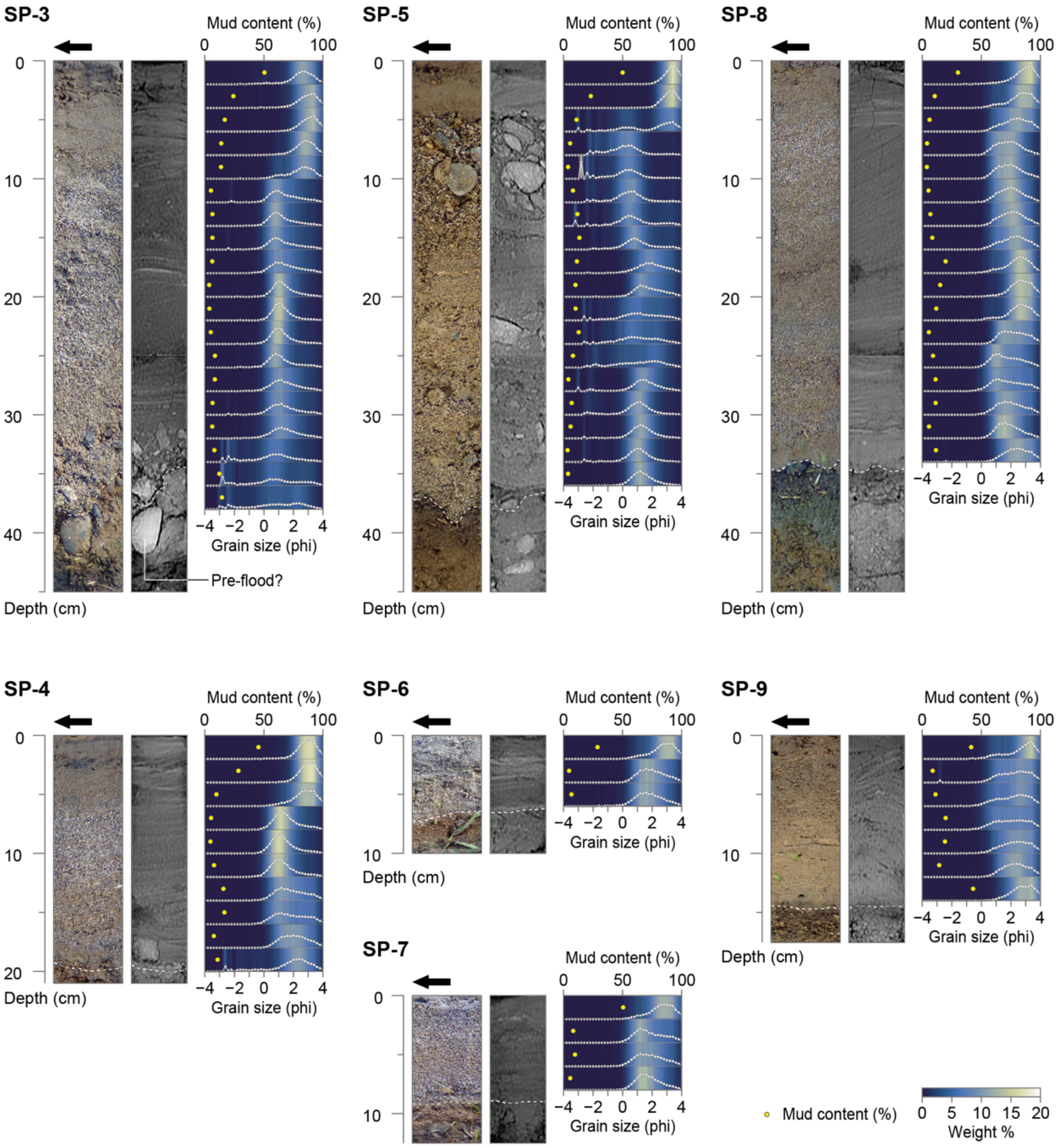

Fig. 14. Photograph (geoslicer sample), CT image, grain size distribution, and mud content (yellow) of crevasse splay deposits in the sandy pile (proximal splay).

Fig. 15. Photographs of crevasse splay deposits at (A) trench A-2 (medial splay), (B) trench E-2 (medial splay), (C) trench A-9 (distal splay), and (D) trench C-4 (distal splay).

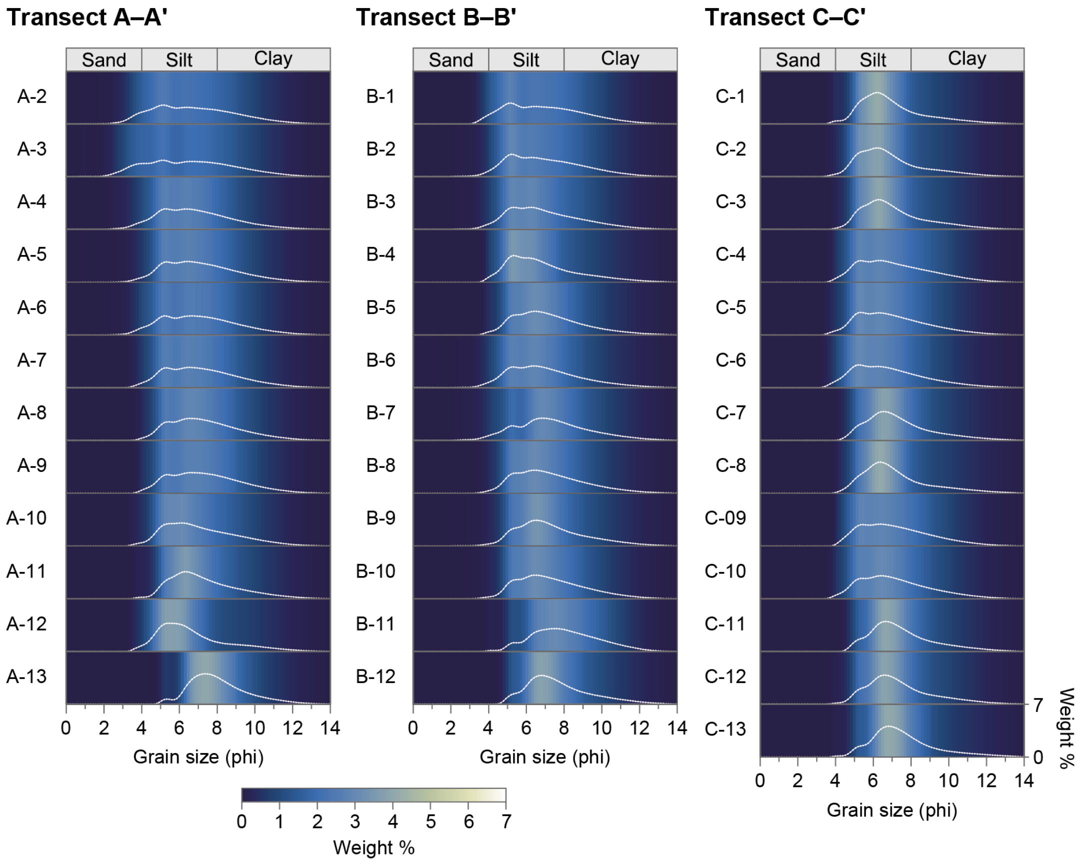

Fig. 16. Grain size distribution of crevasse splay deposits along transects A–A', B–B', and C–C'.

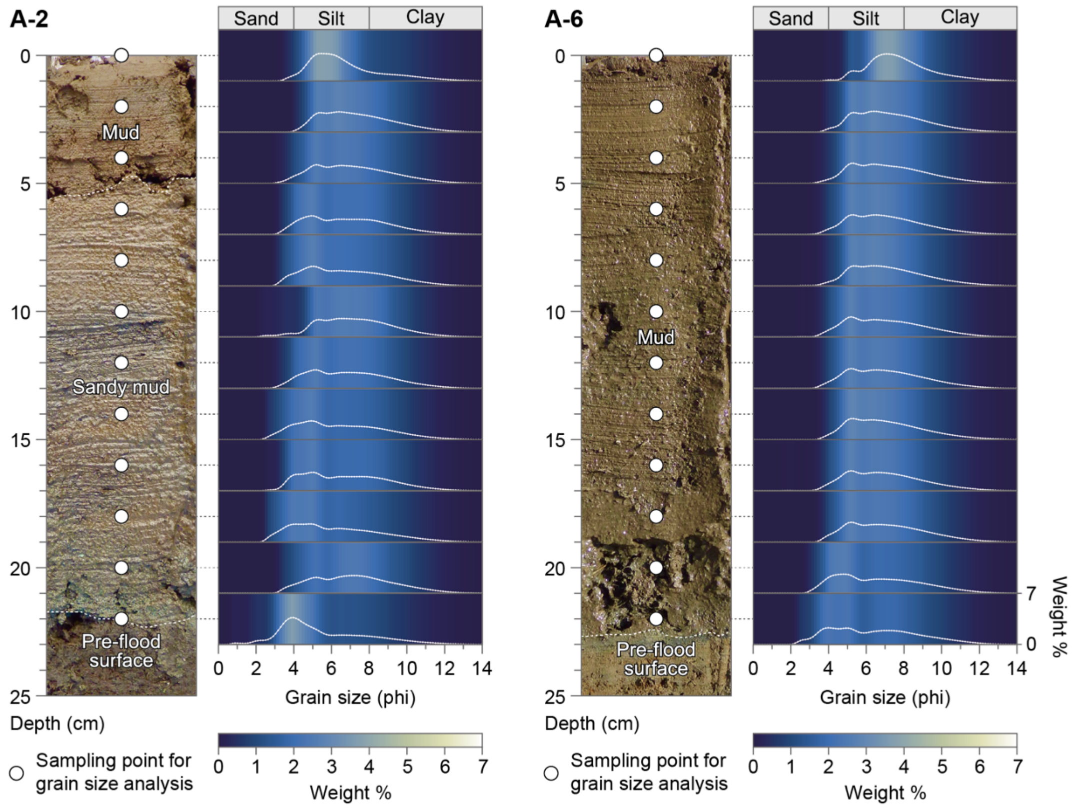

Fig. 17. Vertical change in grain size distribution of the crevasse splay deposits at trenches A-2 (22 cm thick; medial splay) and A-6 (23 cm thick; distal splay).

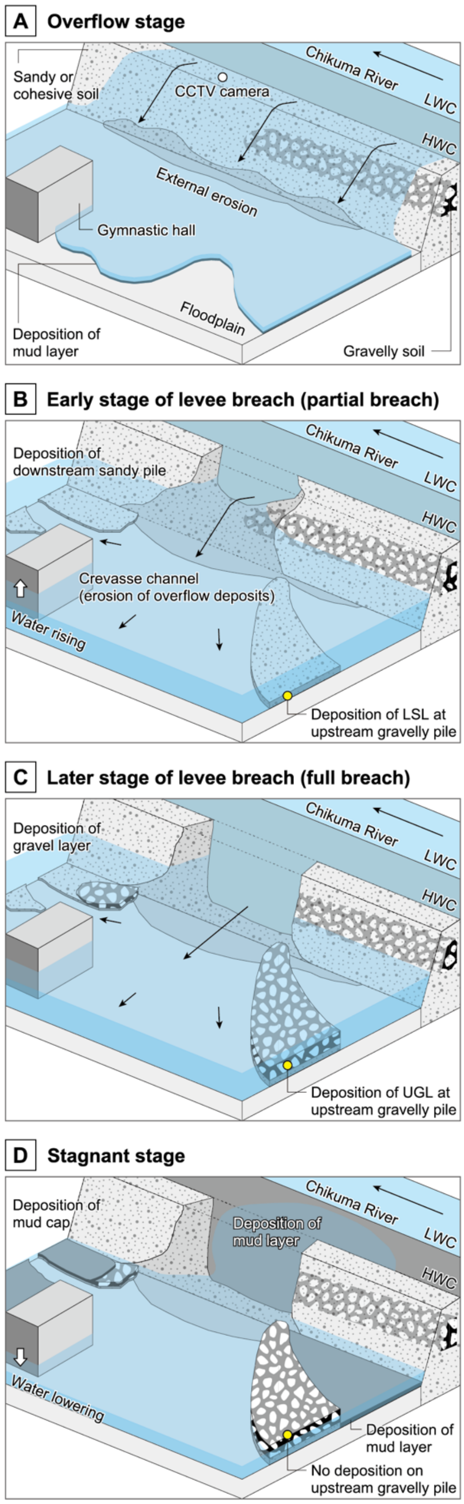

Fig. 18. Reconstruction of sediment transport and deposition processes associated with the levee breaching event: (A) overflow stage, (B) early stage of levee breach (partial breach), (C) later stage of levee breach (full breach), and (D) stagnant stage.

References

Allen, J.R.L., 1965. A Review of the Origin and Characteristics of Recent Alluvial Sediments. Sedimentology 5, 89–191.

Arnaud-Fassetta, G., 2013. Dyke breaching and crevasse-splay sedimentary sequences of the Rhône Delta, France, caused by extreme river-flood of December 2003. Geografia Fisica e Dinamica Quaternaria 36, 7–26.

Bristow, C.S., Skelly, R.L., Ethridge, F.G., 1999. Crevasse splays from the rapidly aggrading, sand-bed, braided Niobrara River, Nebraska: effect of base-level rise. Sedimentology 46, 1029–1047.

Buehler, H.A., Weissmann, G.S., Scuderi, L.A., Hartley, A.J., 2011. Spatial and Temporal Evolution of an Avulsion on the Taquari River Distributive Fluvial System from Satellite Image Analysis. Journal of Sedimentary Research 81, 630–640.

Burns, C.E., Mountney, N.P., Hodgson, D.M., Colombera, L., 2017. Anatomy and dimensions of fluvial crevasse-splay deposits: Examples from the Cretaceous Castlegate Sandstone and Neslen Formation, Utah, U.S.A. Sedimentary Geology 351, 21–35.

Cahoon, D.R., White, D.A., Lynch, J.C., 2011. Sediment infilling and wetland formation dynamics in an active crevasse splay of the Mississippi River delta. Geomorphology 131, 57–68.

Colombera, L., Mountney, N.P., 2021. Influence of fluvial crevasse-splay deposits on sandbody connectivity: Lessons from geological analogues and stochastic modelling. Marine and Petroleum Geology 128, 105060.

Colombera, L., Mountney, N.P., McCaffrey, W.D., 2013. A quantitative approach to fluvial facies models: Methods and example results. Sedimentology 60, 1526–1558.

Falvard, S., Paris, R., Trofimovs, J., 2017. X-ray tomography of tsunami deposits: Towards a new depositional model of tsunami deposits. Sedimentology 64, 453–477.

Farrell, K.M., 2001. Geomorphology, facies architecture, and high-resolution, non-marine sequence stratigraphy in avulsion deposits, Cumberland Marshes, Saskatchewan. Sedimentary Geology 139, 93–150.

Fekete, A., Sandholz, S., 2021. Here Comes the Flood, but Not Failure? Lessons to Learn after the Heavy Rain and Pluvial Floods in Germany 2021. Water 13, 3016.

Fisher, J.A., Krapf, C.B.E., Lang, S.C., Nichols, G.J., Payenberg, T.H.D., 2008. Sedimentology and architecture of the Douglas Creek terminal splay, Lake Eyre, central Australia. Sedimentology 55, 1915–1930.

Folk, R.L., 1966. A review of grain-size parameters. Sedimentology 6, 73–93.

Folk, R.L., Ward, W.C., 1957. Brazos River bar: a study in the significance of grain size parameters. Journal of Sedimentary Research 27, 3–26.

Gębica, P., Sokołowski, T., 2001. Sedimentological interpretation of crevasse splays formed during the extreme 1997 flood in the upper Vistula river valley (South Poland). Annales Societatis Geologorum Poloniae 71, 53–62.

Hori, K., Hirouchi, D., 2011. Crevasse-Splay Deposits of the Asuwa River Valley Plain Caused by the Fukui Heavy Rainfall. Geographical Review of Japan Series A 84, 358–368 (in Japanese with English abstract).

Hughes, D.A., Lewin, J., 1982. A small-scale flood plain. Sedimentology 29, 891–895.

Investigation Committee on the Chikuma River Levee, 2020. A report of the Investigation Committee on the Chikuma River Levee, pp. 1–158. https://www.hrr.mlit.go.jp/river/chikumagawateibouchousa/chikuma-houkokusyo-isshiki.pdf (in Japanese).

Investigation Committee on the Kinu River Levee, 2016. A report of the Investigation Committee on the Kinu River Levee, pp. 1–80. https://www.ktr.mlit.go.jp/ktr_content/content/000643703.pdf (in Japanese).

Ishimura, D., Yamada, K., 2019. Palaeo-tsunami inundation distances deduced from roundness of gravel particles in tsunami deposits. Scientific Reports 9, 10251.

Jones, H.L., Hajek, E.A., 2007. Characterizing avulsion stratigraphy in ancient alluvial deposits. Sedimentary Geology 202, 124–137.

Li, J., Bristow, C.S., 2015. Crevasse splay morphodynamics in a dryland river terminus: Río Colorado in Salar de Uyuni Bolivia. Quaternary International 377, 71–82.

Matsumoto, D., Sawai, Y., Yamada, M., Namegaya, Y., Shinozaki, T., Takeda, D., Fujino, S., Tanigawa, K., Nakamura, A., Pilarczyk, J.E., 2016. Erosion and sedimentation during the September 2015 flooding of the Kinu River, central Japan. Scientific Reports 6, 34168.

Mjøs, R., Walderhaug, O., Prestholm, E., 1993. Crevasse splay sandstone geometries in the Middle Jurassic Ravenscar Group of Yorkshire, UK. In: M. Marzo, C. Puigdefábregas (Eds.), Alluvial Sedimentation. Special Publications of the International Association of Sedimentologists, pp. 167–184.

Nanson, G.C., Croke, J.C., 1992. A genetic classification of floodplains. Geomorphology 4, 459–486.

Nelson, S.A., Leclair, S.F., 2006. Katrina's unique splay deposits in a New Orleans neighborhood. GSA Today 16, 4–10.

O'Brien, P.E., Wells, A.T., 1986. A small, alluvial crevasse splay. Journal of Sedimentary Petrology 56, 876–879.

Ohtsuka, S., Sato, Y., Yoshikawa, T., Sugii, T., Kodaka, T., Maeda, K., 2021. Levee damage and revetment erosion by the 2019 Typhoon Hagibis in the Chikuma River, Japan. Soils and Foundations 61, 1172–1188.

Orlandini, S., Moretti, G., Albertson, J.D., 2015. Evidence of an emerging levee failure mechanism causing disastrous floods in Italy. Water Resources Research 51, 7995–8011.

Özer, I.E., van Damme, M., Jonkman, S.N., 2019. Towards an International Levee Performance Database (ILPD) and Its Use for Macro-Scale Analysis of Levee Breaches and Failures. Water 12, 119.

Pérez-Arlucea, M., Smith, N.D., 1999. Depositional patterns following the 1870s avulsion of the Saskatchewan River (Cumberland Marshes, Saskatchewan, Canada). Journal of Sedimentary Research 69, 62–73.

Rahman, M.M., Howell, J.A., MacDonald, D.I.M., 2022a. Quantitative analysis of crevasse-splay systems from modern fluvial settings. Journal of Sedimentary Research 92, 751–774.

Rahman, M.M., Howell, J.A., Macdonald, D.I.M., 2022b. Virtual outcrop-based analysis of channel and crevasse splay sandstone body architecture in the Middle Jurassic Ravenscar Group, Yorkshire, NE England. Journal of the Geological Society 179, jgs2021-2017.

Sato, Y., Miyachi, Y., Urabe, A., Komatsubara, J., Naya, T., 2017. Crevasse splay deposits of the 2015 Kanto-Tohoku Torrential Rain Disaster in the central part of the Kinu River, Kami-Misaka district, Joso City. The Quaternary Research (Daiyonki-Kenkyu) 56, 37–50 (in Japanese with English abstract).

Shakti, P.C., Kamimera, H., Misumi, R., 2020. Inundation Analysis of the Oda River Basin in Japan during the Flood Event of 6–7 July 2018 Utilizing Local and Global Hydrographic Data. Water 12, 1005.

Smith, N.D., Cross, T.A., Dufficy, J.P., Clough, S.R., 1989. Anatomy of an avulsion. Sedimentology 36, 1–23.

Takada, K., Nakata, T., Miyagi, T., Haraguchi, T., Nishitani, Y., 2002. Handy Geoslicer – New soil sampler for Quaternary geologist. Chishitsu News 579, 12–18 (in Japanese).

Tinh, N.X., Tanaka, H., Abe, G., Okamoto, Y., Pakoksung, K., 2021. Mechanisms of Flood-Induced Levee Breaching in Marumori Town during the 2019 Hagibis Typhoon. Water 13, 244.

Toonen, W.H.J., van Asselen, S., Stouthamer, E., Smith, N.D., 2016. Depositional development of the Muskeg Lake crevasse splay in the Cumberland Marshes (Canada). Earth Surface Processes and Landforms 41, 117–129.

Tsuchiya, M., 2021. River embankment damage and management along the Chikuma River due to Typhoon No. 19 in October 2019. Journal of Japan Society for Natural Disaster Science 40, 191–212 (in Japanese with English abstract).

Viero, D.P., D'Alpaos, A., Carniello, L., Defina, A., 2013. Mathematical modeling of flooding due to river bank failure. Advances in Water Resources 59, 82–94.

Wessel, P., Luis, J.F., Uieda, L., Scharroo, R., Wobbe, F., Smith, W.H.F., Tian, D., 2019. The Generic Mapping Tools Version 6. Geochemistry, Geophysics, Geosystems 20, 5556–5564.

Widera, M., Chomiak, L., Wachocki, R., 2023. Distinct types of crevasse splays formed in the area of Middle Miocene mires, central Poland: Insights from geological mapping and facies analysis. Sedimentary Geology 443, 106300.

Yamamoto, H., Watanabe, Y., Kanemitsu, N., Miyakawa, Y., Ohtani, Y., Sakamoto, K., Iwaya, K., 2020. Damage Investigation of Flood Disaster in Nagano City by Typhoon No.19 (hagibis) in 2019. Journal of Japan Society for Natural Disaster Science 39, 221–252 (in Japanese with English abstract).